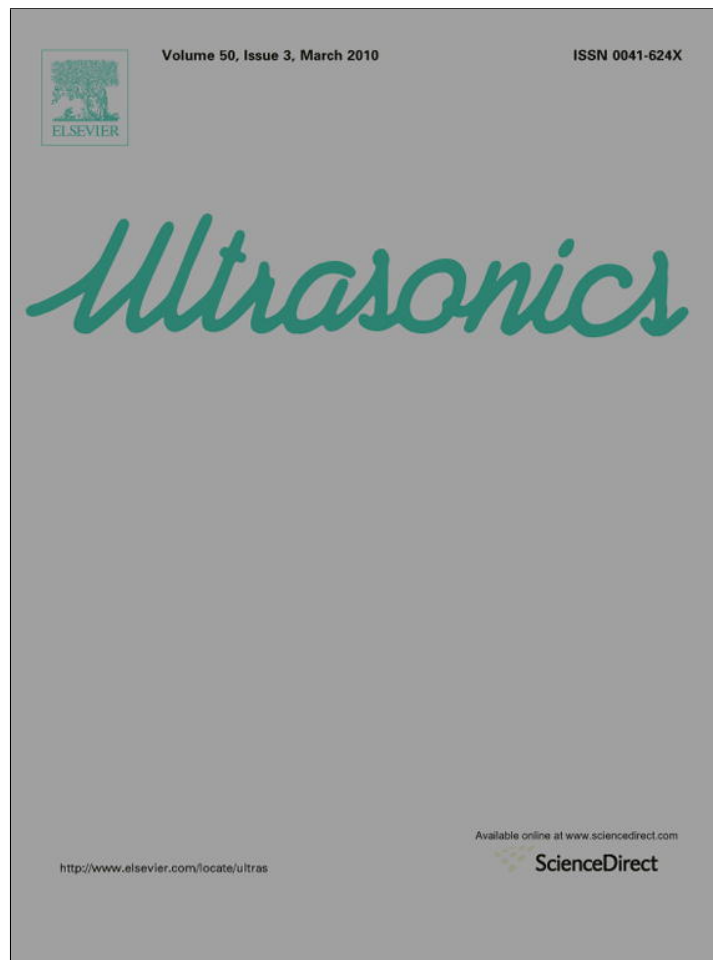


Provided for non-commercial research and education use.
Not for reproduction, distribution or commercial use.



This article appeared in a journal published by Elsevier. The attached copy is furnished to the author for internal non-commercial research and education use, including for instruction at the authors institution and sharing with colleagues.

Other uses, including reproduction and distribution, or selling or licensing copies, or posting to personal, institutional or third party websites are prohibited.

In most cases authors are permitted to post their version of the article (e.g. in Word or Tex form) to their personal website or institutional repository. Authors requiring further information regarding Elsevier's archiving and manuscript policies are encouraged to visit:

<http://www.elsevier.com/copyright>

Contents lists available at [ScienceDirect](http://www.sciencedirect.com)

Ultrasonics

journal homepage: www.elsevier.com/locate/ultras

Analysis of motion tracking in echocardiographic image sequences: Influence of system geometry and point-spread function

Basma Touil*, Adrian Basarab, Philippe Delachartre, Olivier Bernard, Denis Friboulet

CREATIS, CNRS UMR 5520, INSERM U 630, INSA-Lyon F-69621, France

ARTICLE INFO

Article history:

Received 28 April 2009

Received in revised form 6 August 2009

Accepted 7 September 2009

Available online 19 September 2009

Keywords:

Echography

Motion estimation

Decorrelation

Block matching

Bilinear deformable block matching

Cardiac motion

Echocardiography

ABSTRACT

This paper focuses on motion tracking in echocardiographic ultrasound images. The difficulty of this task is related to the fact that echographic image formation induces decorrelation between the underlying motion of tissue and the observed speckle motion. Since Meunier's seminal work, this phenomenon has been investigated in many simulation studies as part of speckle tracking or optical flow-based motion estimation techniques. Most of these studies modeled image formation using a linear convolution approach, where the system point-spread function (PSF) was spatially invariant and the probe geometry was linear. While these assumptions are valid over a small spatial area, they constitute an oversimplification when a complete image is considered. Indeed, echocardiographic acquisition geometry relies on sectorial probes and the system PSF is not perfectly invariant, even if dynamic focusing is performed.

This study investigated the influence of sectorial geometry and spatially varying PSF on speckle tracking. This was done by simulating a typical 64 elements, cardiac probe operating at 3.5 MHz frequency, using the simulation software Field II. This simulation first allowed quantification of the decorrelation induced by the system between two images when simple motion such as translation or incompressible deformation was applied. We then quantified the influence of decorrelation on speckle tracking accuracy using a conventional block matching (BM) algorithm and a bilinear deformable block matching (BDBM) algorithm. In echocardiography, motion estimation is usually performed on reconstructed images where the initial sectorial (i.e., polar) data are interpolated on a cartesian grid. We therefore studied the influence of sectorial acquisition geometry, by performing block matching on cartesian and polar data.

Simulation results show that decorrelation is spatially variant and depends on the position of the region where motion takes place relative to the probe. Previous studies did not consider translation in their experiments, since their simulation model (spatially invariant PSF and linear probe) yields by definition no decorrelation. On the opposite, our realistic simulation settings (i.e., sectorial probe and realistic beamforming) show that translation yields decorrelation, particularly when translation is large (above 6 mm) and when the moving regions is located close to the probe (distance to probe less than 50 mm).

The tracking accuracy study shows that tracking errors are larger for the usual cartesian data, whatever the estimation algorithm, indicating that speckle tracking is more reliable when based on the unconverted polar data: for axial translations in the range 0–10 mm, the maximum error associated to conventional block matching (BM) is 4.2 mm when using cartesian data and 1.8 mm for polar data. The corresponding errors are 1.8 mm (cartesian data) and 0.4 mm (polar data) for an applied deformation in the range 0–10%. We also show that accuracy is improved by using the bilinear deformable block matching (BDBM) algorithm. For translation, the maximum error associated to the bilinear deformable block matching is indeed 3.6 mm (cartesian data) and 1.2 mm (polar data). Regarding deformation, the error is 0.7 mm (cartesian data) and 0.3 mm (polar data). These figures also indicates that the larger improvement brought by the bilinear deformable block matching over standard block matching logically takes place when deformation on cartesian data is considered (the error drops from 1.8 to 0.7 mm in this case).

We give a preliminary evaluation of this framework on a cardiac sequence acquired with a Toshiba Powervision 6000 imaging system using a probe operating at 3.25 MHz. As ground truth reference motion is not available in this case, motion estimation performance was evaluated by comparing a reference image (i.e., the first image of the sequence) and the subsequent images after motion compensation has been applied. The comparison was quantified by computing the normalized correlation between the

* Corresponding author. Tel.: +33 472 43 87 81; fax: +33 472 43 85 26.

E-mail address: basma.touil@creatis.insa-lyon.fr (B. Touil).

reference and the motion-compensated images. The obtained results are consistent with the simulation data: correlation is smaller for cartesian data, whatever the estimation algorithm. The correlation associated to the conventional block matching (BM) is in the range 0.45–0.02 when using cartesian data and in the range 0.65–0.2 for polar data. The corresponding correlation ranges for the bilinear deformable block matching are 0.98–0.2 and 0.98–0.55. In the same way these figures indicate that the bilinear deformable block matching yield a larger improvement when cartesian data are considered (correlation range increases from 0.45–0.02 to 0.98–0.2 in this case).

© 2009 Elsevier B.V. All rights reserved.

Contents

1. Introduction	374
2. Echographic image simulation	375
2.1. Ultrasound simulation model	375
2.2. The probe	375
2.3. The tissue	376
3. Applied motions	377
4. Motion tracking	377
4.1. Block matching (BM)	377
4.2. Bilinear deformable block matching	377
4.2.1. Bilinear motion model	377
4.2.2. Motion estimation algorithm	377
4.3. Polar versus cartesian block matching	378
5. Quantification of motion tracking reliability	378
5.1. Correlation measure	378
5.2. Motion accuracy	378
6. Simulation results	378
6.1. Decorrelation	378
6.1.1. Translation	378
6.1.2. Deformation	379
6.2. Motion estimation accuracy	379
6.2.1. Translation	379
6.2.2. Deformation	380
7. Results from echocardiographic data	383
8. Conclusion	383
References	385

1. Introduction

Motion estimation of the left ventricle is a valuable tool for assessing cardiac function. Special attention has been paid to motion analysis in echocardiography, because of its high temporal resolution and its relatively low cost. However, the analysis of echocardiographic images is generally difficult because of the complexity of the echographic image formation process. Echographic images result from the elementary signals backscattered by the biological scatterers contained in theinsonified tissue. Since the ultrasonic probe records the coherent sum of these signals, the image can be seen as resulting from an interference scheme, producing the speckle patterns commonly observed in ultrasound imaging. While speckle patterns are often regarded as noise (i.e., for tasks such as segmentation), they are used as information for motion estimation, since they provide natural tokens linked to the local configuration of scatterers in the tissue explored.

As a consequence, many approaches have been described that use this feature to estimate motion from echocardiographic image sequences. One of the first types of approaches described in the literature is based on the differential technique known as optical flow [1–3]. Since they rely on the local analysis of spatial and temporal gradients, these methods may fail at estimating large inter-frame cardiac motion. This implies multiscale strategies or a first stage of block-matching to provide a reliable displacement estimate [4–6]. Another approach estimates cardiac motion by performing speckle tracking, which is generally done by comparing a block in the reference image and a block in the subsequent deformed im-

age through a similarity measure such as cross-correlation (CC) [4,5,7], the sum of absolute differences (SAD) [8] or the sum of squared differences (SSD) [9]. An interesting interpretation of these measures has been given by Strintzis [10], who formulated block matching as the maximum likelihood estimation of motion between blocks of known statistics. Maximum likelihood motion estimation is then shown to correspond to the maximization of SAD for Laplacian statistics and SSD in the case of Gaussian statistics. Using this framework, a new similarity measure was derived when the image was described through a multiplicative noise with a Rayleigh density. This line of reasoning has been pursued by Cohen [11], Boukerroui [12] and Linguraru [13], who incorporated this similarity measure for block matching.

The above-described approaches were based on conventional envelope-detected images, obtained through demodulation of the ultrasound radiofrequency (RF) signals. Some studies have proposed performing speckle tracking by using the RF signal to evaluate small displacements. Since the RF signal contains much higher frequencies, it is indeed better adapted to the estimation of small-scale motion (typically on the order of the emitted pulse wavelength). Examples of this type of study include the work by Lubinski [14] and more recently by D'hooge [15], who used speckle tracking to estimate the strain or strain rate in the myocardium. RF-based speckle tracking is, however, currently not widespread in the field of echocardiography because its high motion sensitivity implies high frame rates [15,16] and the difference in resolution in the propagation and transverse directions makes the 2D estimation of motion difficult. This extension to 2D is a challenge in terms of

processing [14,17–19] and US image formation [20]. An interesting comparison between envelope-detected and RF-based echocardiographic speckle tracking has recently been made by Yu et al. [21].

Speckle tracking methods are based on the assumption that the motion of the speckle patterns reliably reflects the motion of the tissue, i.e., of the underlying scatterers. Since echographic image formation is essentially the interference process described above, this assumption does not hold whenever the tissue motion is large enough to modify the geometrical configuration of scatterers as “seen” by the probe, thereby changing the shape of the speckle patterns.¹ This yields what is known as motion decorrelation, i.e., a difference between the apparent motion present in the image and the real motion of the tissue. In echocardiography, this phenomenon is directly related to the temporal sampling rate (a low sampling rate yields large inter-frame motion) and to the specific, sectorial geometry of the probe: a simple translation changes the speckle pattern received by the probe. It should also be noted that a further consequence of sectorial geometry lies in the fact that it yields a sparser lateral sampling far from the probe.

Since Meunier’s influential work [22], the influence of decorrelation on motion estimation has been recognized and many studies describe strategies to minimize its influence such as temporal stretching [23], the Lagrangian model of speckle [24], signal compounding [25], deformable block matching [26], multiscale strategies [27] and nonlinear filtering [6].

In this context, it should be noted that the validation of the motion tracking techniques proposed in the above-mentioned literature very often stems from numerical simulations aiming at estimating their accuracy [1,7,9,13,19,24,25] and the influence of decorrelation [21,22] by comparing the simulated and the estimated motion. In the specific field of motion tracking from echocardiographic images, the simulations used to validate the motion estimation approaches [1,7,13,19,21,22] suffer from two major limitations. First, echographic image formation is modeled as a linear convolution, where the ultrasonic system point-spread function (PSF) is invariant in space. While this assumption is valid over a small spatial area, it is an oversimplification since the PSF system is not perfectly invariant throughout the entire image, even with dynamic focusing. These studies introduce a further simplification by considering linear probe geometry, although sectorial probes are used in echocardiography, in order to have acoustic access to the heart between the ribs. One notable exception to these limitations is the study conducted by Langeland [28], which used a specific simulation environment and sectorial acquisition geometry to compare displacement estimators for motion tracking, such as correlation, SSD and SAD. However, this study was conducted in the particular context of RF-based motion estimation using very high frame rates (500 Hz) and a reduced sector (15°).

In this context, the main goal of this paper is to report the study of the influence of decorrelation and sectorial geometry on the accuracy of motion tracking through realistic simulation, using conventional echocardiographic acquisition settings (i.e., large acquisition sector and motion magnitudes corresponding to the usual sampling rates). The simulation is based on the Field II simulation software, which provides an efficient tool to simulate ultrasound fields by incorporating realistic transducer features and allows for beam forming, dynamic focusing, apodization and sectorial geometry. To clarify the influence of decorrelation on speckle tracking, we studied simple 2D affine motions such as translation and incompressible deformation (i.e., we did not study the decorrelation related to out-of-plane motion). This influence was quantified by evaluating the inter-frame correlation and the resulting

motion estimation accuracy, using conventional SAD-based block matching (BM). We also examined whether a more sophisticated tracking algorithm such as deformable block matching (DBBM) [29] can minimize the influence of decorrelation and improve the accuracy obtained. Given the sectorial geometry of acquisition, the initial data set corresponds to a rectangular grid in polar coordinates. The conventional echographic image is usually reconstructed from these polar data by conversion and interpolation on cartesian coordinates. To further explore the influence of sectorial acquisition geometry, the block matching methods were applied to cartesian and polar data. This framework was then applied to real echocardiographic data. As ground truth reference motion is not available for these data, motion estimation is evaluated by comparing a given reference image and the subsequent image after motion compensation.

The paper is structured as follows: Section 2 describes the simulation model with the corresponding parameters of the probe and tissue and Section 3 details the motion applied to this tissue. Section 4 describes the motion tracking methods, i.e., block matching (BM) and bilinear deformable block matching (DBBM). Section 5 presents the measures used to quantify decorrelation and motion estimation accuracy. The simulation results are provided and analyzed in Section 6. Section 7 provides the results obtained from real echocardiographic data. The paper is concluded in Section 8.

2. Echographic image simulation

2.1. Ultrasound simulation model

Most of the previous studies using simulations to assess motion estimation in echocardiography [1,7,13,19,21,22] have used the linear system-based model initially proposed by Meunier to generate US images. In this approach, the RF signal is obtained as a convolution between the PSF representing the system and a set of tissue scatterers in the far field. However, this model is valid only locally and cannot properly model the acquisition performed with a real echographic device, which involves beam forming (allowing dynamic focusing), apodization and sectorial geometry.

This led us to simulate US images using Field II [30], which provides an efficient tool to simulate ultrasound fields by incorporating realistic transducer features. The Field software uses the concept of spatial impulse responses as developed by Tupholme and Stepanishen [31,32], including the excitation scheme (dynamic focusing and apodization). This approach determines the ultrasound field at any point in space as a function of time for any type of excitation. The impulse response obtained varies as a function of position relative to the transducer. As a consequence, the simulated acquisition set-up can be seen as a system with a spatially variant PSF.

One limitation of this framework is linked to the fact that Field II does not allow for simulating non linear wave propagation, such as second harmonic imaging which is now frequently used in clinical practice. The conclusions drawn from the simulations should therefore be restricted to conventional fundamental imaging acquisitions.

2.2. The probe

The simulation requires choosing the parameters defining the probe. We used a typical cardiac probe whose parameters are given in Table 1. These parameters are used to simulate acquisitions with a sectorial probe to take into account the influence of the probe geometry on the echographic images.

The output of a simulation consists in the RF image of the tissue explored. The B-mode images are obtained as the logarithm of the Hilbert transform of the resulting RF signal.

¹ A simple illustrative example of this problem is a tissue undergoing a simple rigid-body rotation and imaged with a linear probe [22].

Table 1
The simulation parameters.

Parameters	Value
Transducer frequency	3.5 MHz
Sound speed in tissue	1540 m/s
Wavelength	0.256 mm
Sampling frequency	33 MHz
Dynamic focusing distance	(40 mm, 50 mm, 60 mm... 120 mm)
Angle of increment	0.7°
Number of active elements	64
Number of lines	128
Element height	14 mm
Pitch (distance between two consecutive elements center)	0.3 mm
Kerf (space between two consecutive elements)	0.05 mm
Elevation focus	67 mm

To show the spatially variant nature of the PSF, we simulated the ultrasound image of 22 point scatterers positioned along the central axis of the probe (Fig. 1a), with the scatterers 5 mm apart. The resulting image (Fig. 1b) shows how the impulse response depends on the location in the image.

This phenomenon may be further quantified by computing the correlation between the PSF at the focus position ($D = 67$ mm) and

the PSF at other depths, as shown in Fig. 1c. The correlation value is one at the focus distance and decreases on both sides, especially in near field (closer to the probe).

2.3. The tissue

Echocardiographic data acquired from the myocardium region corresponds to fully developed speckle, resulting in Rayleigh statistics for the envelope-detected image as shown by Meunier and Yu [21,22]. We simulated such conditions as follows. The simulated tissue is modelled by a collection of individual point scatterers. Each scatterer is defined through its x - y coordinates and scattering coefficient. The distribution of scatterers can then be expressed as

$$d(x,y) = \sum_{i=1}^N A(i)\delta(x - x_i, y - y_i)$$

where N is the total number of scatterers in the simulated tissue, $A(i)$ is the scattering coefficient of the i th scatterer, (x_i, y_i) are its spatial coordinates and δ the delta function.

When the scatterers density is high (i.e., N is large) and the spatial coordinates follow a uniform distribution, this model yields fully developed speckle and Rayleigh statistics for the envelope signal [33].

In our simulation, the tissue was simulated as a 20 mm × 5 mm rectangular region containing $N = 1000$ point scatterers. A uniform

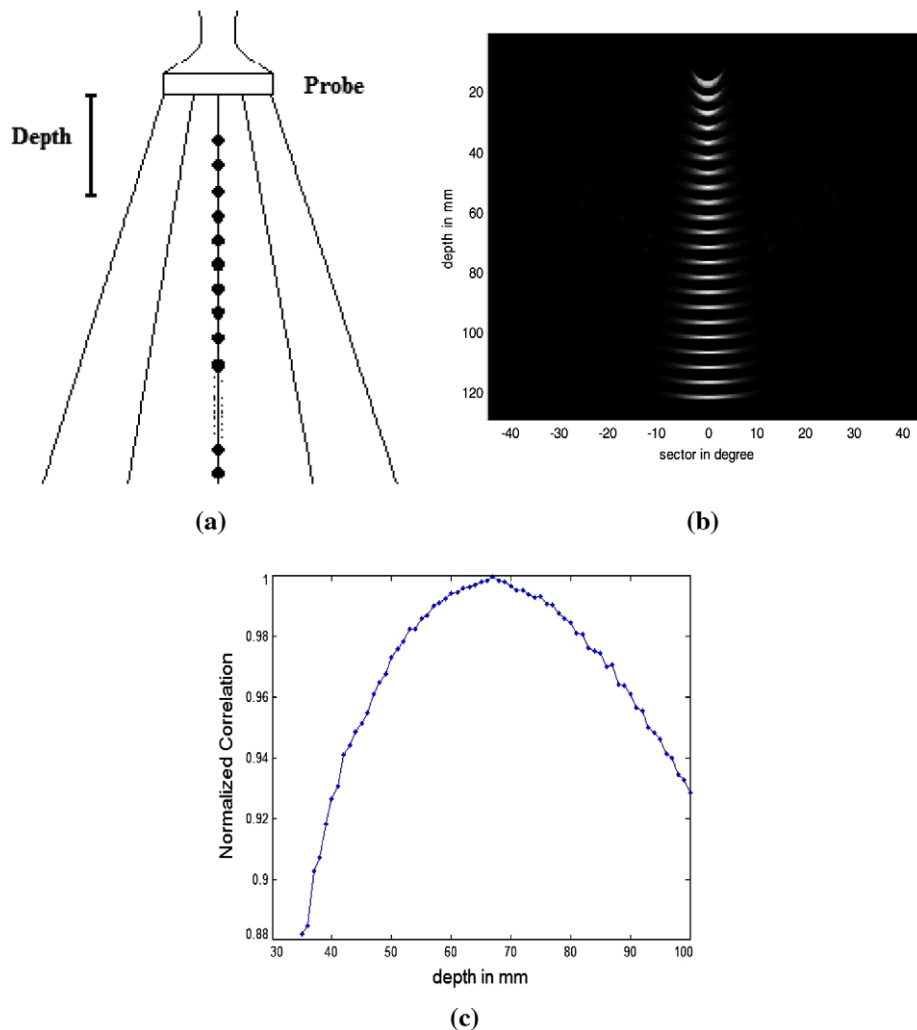


Fig. 1. (a) Location of the scatterers along the central axis of the probe. (b) Corresponding simulated image. (c) Correlation between PSF at the focus zone and the PSFs at other depths.

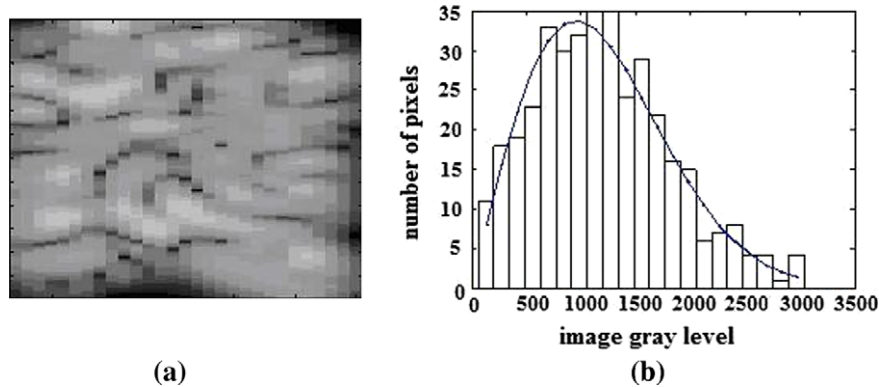


Fig. 2. (a) B-mode image of the simulated tissue. (b) Histogram of the B-mode image and the fitted Rayleigh distribution. The solid rectangles correspond to the histogram of the image while the blue curve corresponds to the Rayleigh distribution fitted to the image data. (For interpretation of the references to colour in this figure legend, the reader is referred to the web version of this article.)

random generator was used to generate the spatial coordinates (x_i, y_i) within the region. In the same way, a Gaussian distribution was used to select the scattering cross-section $A(i)$ of each scatterer.

Fig. 2a displays an example of a simulated image. Fig. 2b shows the histogram of this image and the fit of a Rayleigh distribution computed from the image data, using the maximum likelihood estimator. The quality of this fit shows that our settings yield the desired fully developed speckle conditions.

3. Applied motions

The first experiment consisted in a simple axial translation (i.e., along the central axis of the probe). This motion transformation was a useful reference in this study. This motion model had not been considered in previous studies [21,22]: their use of a linear system-based model implies by definition that translation yields no decorrelation. A recent paper [34] showed that even with a linear probe a decorrelation occurs for a simple translation. This decorrelation increases with the sectorial geometry of the probe. The second motion studied consisted in an axial deformation with an incompressibility constraint (i.e., axial dilation and lateral compression) centered on the tissue. The translation was performed in the range of 0–10 mm, as in [15,21,22], the deformation was applied from 0 to 10%. Note that to assess the influence of PSF variation and probe geometry on motion estimation; these experiments were conducted for different depths D of the region relative to the probe, as shown in Fig. 1a.

4. Motion tracking

4.1. Block matching (BM)

For each block, a motion vector was estimated as the one that maximized a measure criterion, which typically is either the sum of squared difference (SSD) or sum of absolute difference (SAD). Here we chose the SAD as a similarity measure and the velocity vector (dx, dy) that yields the best fit between image regions at different times as:

$$\begin{aligned} \text{SAD}(x, y, dx, dy) \\ = \sum_{i=-n}^n \sum_{j=-m}^m |I_1(x+i, y+j) - I_2(x+i+dx, y+j+dy)| \end{aligned} \quad (1)$$

where I_1 and I_2 are the corresponding image regions, $2 \times n$ and $2 \times m$ are, respectively, the lateral and axial size of region of interest and (x, y) the position of the node around what the SAD was computed.

4.2. Bilinear deformable block matching

The method referred to as a bilinear deformable block matching (BDBM) [35,36] was developed for ultrasound applications to improve motion tracking, as compared to conventional block matching. This iterative approach uses a local bilinear model with eight parameters for controlling the local mesh deformation. We briefly outline this method hereafter.

4.2.1. Bilinear motion model

A bilinear model was chosen to describe the local displacement. The components of the motion vector are formulated as follows:

$$u(x, y) = a_u \cdot x + b_u \cdot y + c_u \cdot x \cdot y + d_u \quad (2)$$

$$v(x, y) = a_v \cdot x + b_v \cdot y + c_v \cdot x \cdot y + d_v \quad (3)$$

where u and v are, respectively, lateral and axial displacements at each position (x, y) .

In this context, we need to estimate the eight parameters of the bilinear model to estimate local displacement.

4.2.2. Motion estimation algorithm

The parameters of the bilinear motion model are estimated in rectangular regions of interest (ROI R (hatched region in Fig. 3), chosen around the defined nodes N . They are estimated by estimating the translations of the four corners (noted C_i) of this region of interest. Corner translations are estimated considering rectangular blocks (noted B_i) centered on each corner and joined in the current node N . Simple block matching is then used to estimate these four 2-D translations. In Fig. 3, an asterisk denotes the nodes, corners and blocks after the local spatial transformation.

The estimation of these four translations of corners allows estimating the parameters of the bilinear model. This algorithm works iteratively with a multiscale approach. At each resolution level, the computation grid is refined by bilinear interpolation. At each iteration, the current study zone of the initial image is deformed using the bilinear parameters estimated at the previous iteration. In this way, the next iteration starts with four deformed blocks, which allow better estimation of the current region of interest's corner translations. The iterative multiscale approach has the advantage of decreasing motion error with the advancement of iterations.

Experiments conducted by [35] demonstrated that an interpolation factor of 3 at two iterations for the BDBM provide a better compromise between motion estimation accuracy and estimation time. In our study, we decided to compute the BM with an interpo-

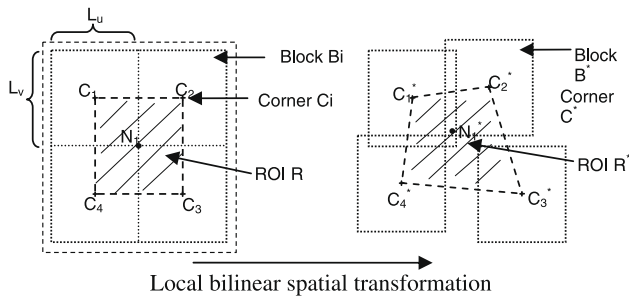


Fig. 3. Scheme of the bilinear spatial transformation applied to the block where bilinear deformable block matching is performed.

lation factor of 9, which finally corresponds to an interpolation of 3 at two iterations for the BDBM.

4.3. Polar versus cartesian block matching

Because of the sectorial geometry of acquisition, the initial data set corresponds to a rectangular grid in polar coordinates. The conventional echographic image is usually reconstructed from these polar data by conversion and interpolation on cartesian coordinates. As sketched in Fig. 4, when block matching is performed, a rectangular block contains less information (i.e., fewer lines from the original polar data) far from the probe, which influences the accuracy of motion estimation as a function of depth.

This situation can be improved by performing block matching with rectangular blocks directly on the initial polar data (Fig. 4a). By doing so, the quantity of information in a block is the same at any depth. In cartesian coordinates, performing block matching is equivalent to using fan-shaped, adaptive blocks (Fig. 4c).

These two block matching schemes were used in the experiments.

5. Quantification of motion tracking reliability

5.1. Correlation measure

We used the normalized correlation to quantify the difference between apparent and real motion. An initial image I_0 was simulated using the initial position of the scatterers (i.e., “before” motion). A motion transformation T was then applied to I_0 , yielding the image I_1 . I_1 was used as a reference image, since it corresponds to the image that would be obtained if no decorrelation occurred. We then applied the same motion transformation T directly to the scatterers from which a second image I_2 was generated, corre-

sponding to the “real” echographic image after motion. Comparing I_1 and I_2 makes it possible to measure the decorrelation induced by motion.

Since the data obtained by Field II in the example of a sectorial probe are in polar coordinates, we used the normalized correlation in polar coordinates (r, θ) , i.e.:

$$corr = \frac{\sum_{\Omega} \sum_{\Omega} (I_1(r, \theta) - \bar{I}_1) \times (I_2(r, \theta) - \bar{I}_2)}{\sqrt{\sum_{\Omega} (I_1(r, \theta) - \bar{I}_1)^2} \times \sqrt{\sum_{\Omega} (I_2(r, \theta) - \bar{I}_2)^2}} \quad (4)$$

where \bar{I}_1 and \bar{I}_2 are the grayscale means of I_1 and I_2 .

In our study, the normalized correlation was computed on Ω = (two-resolution cell-size region), corresponding to a 1.2×2.5 -mm tissue region.

5.2. Motion accuracy

Accuracy was assessed by comparing the estimated motion and the true motion applied to the scatterers. At each image point, we computed the absolute error vector as the difference between the true and estimated velocity vectors. We computed this error on $N = 50$ tissues. For each experiment, the mean of the error vector magnitude (called MEM) and the associated standard deviation (SDEM) are reported.

Defining $v_{est}(T)$ and $v_{true}(T)$ as the estimated and true motion vector at the experiment T , the error is given as:

$$Err(T) = |v_{est}(T) - v_{true}(T)| \quad (5)$$

We then have

$$MEM = \frac{\sum_{T=1}^N Err(T)}{N} \quad (6)$$

and

$$SDEM = \sqrt{\frac{\sum_{T=1}^N (Err(T) - MEM)^2}{N}} \quad (7)$$

6. Simulation results

6.1. Decorrelation

6.1.1. Translation

Fig. 5 qualitatively illustrates the influence of decorrelation as a function of translation magnitude. Fig. 5a shows the speckle patterns of the image corresponding to the tissue initial position, while Fig. 5b and c shows the images corresponding to a 2 mm and a 10 mm translation applied to the tissue, respectively. For a better interpretation of the images, a well-defined speckle pattern

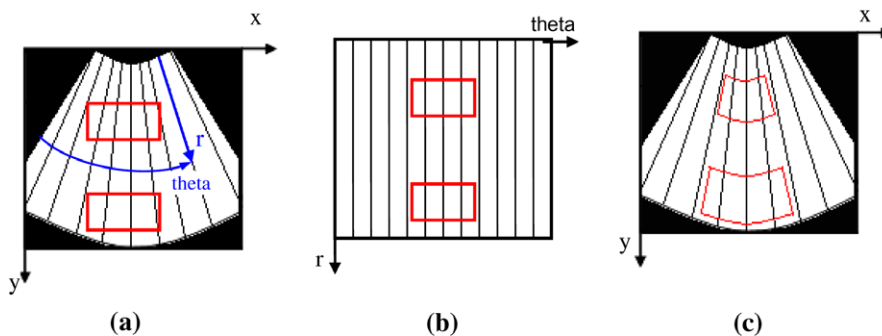


Fig. 4. (a) Geometry of the block matching method when applied on the reconstructed image in cartesian coordinates. (b) Geometry of the block matching method when applied to polar data, represented in polar coordinates. (c) Geometry of the block matching method when applied to polar data represented in cartesian coordinates.

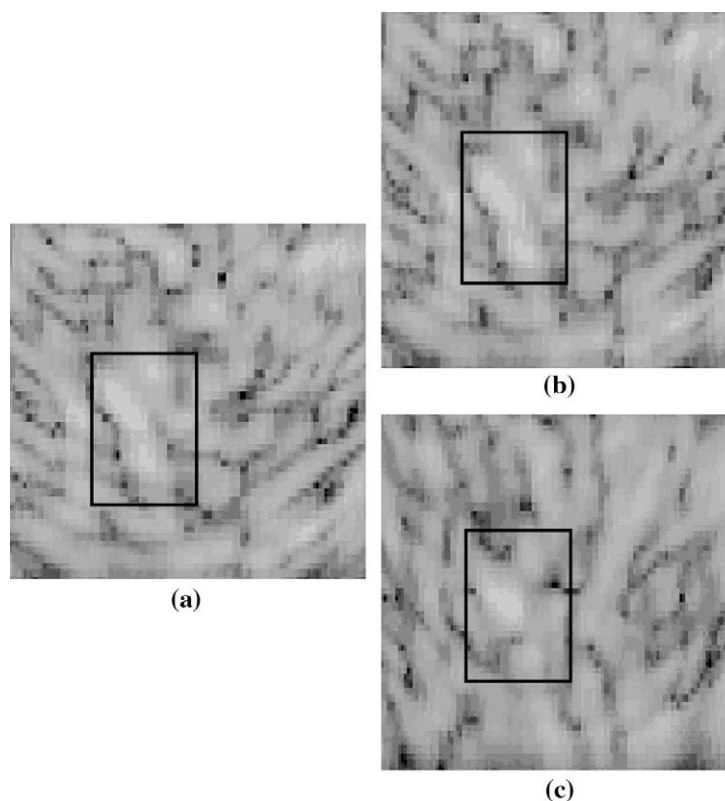


Fig. 5. Simulated polar image corresponding to the tissue in initial position. A well-defined speckle pattern is designated by the black rectangle. (b) Image obtained after a 2 mm translation has been applied to the tissue. Decorrelation is very low and the initial speckle pattern may be easily tracked. (c) Image obtained after a 10 mm translation has been applied to the tissue. Because the translation is larger, important decorrelation takes place and the initial speckle pattern is almost lost.

has been isolated by a black rectangle in the initial image on Fig. 5a. Because a 2 mm translation yields a weak decorrelation, this speckle pattern may be easily recognized in the corresponding rectangle on Fig. 5b. On the opposite, the larger translation corresponding to Fig. 5b yields a stronger decorrelation and the speckle structure is almost completely lost.

The correlation between the reference image and the image corresponding to motion was computed as described in Section 5.1. The results obtained are plotted in Fig. 6 for different translation magnitudes and for different depths D of the region relative to the probe. Fig. 6 shows that the correlation coefficient decreased when the translation magnitude increased. This behavior is clearly more pronounced when the tissue is located near the probe. This phenomenon is consistent with the observation made from

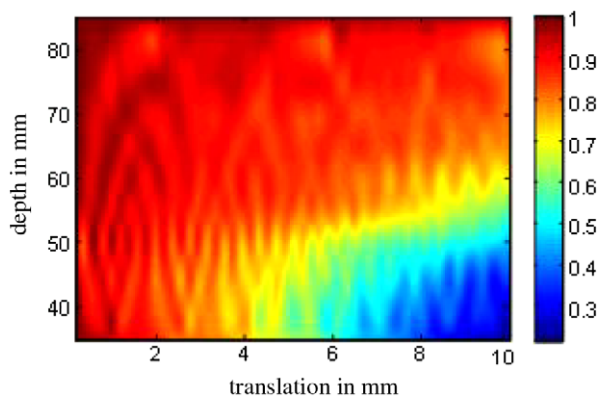


Fig. 6. Normalized correlation for the translation, as a function of depth from the probe and translation magnitude.

Fig. 1c: because of the rapid variation of the PSF near the probe, a tissue located in this area and experiencing translation is “seen” with two different PSFs, inducing the observed decorrelation.

On the contrary, this problem is quite insignificant given that the insonified tissue was far enough from the probe: even for large translations, the correlation showed satisfying values beyond 65 mm.

6.1.2. Deformation

The results obtained for deformation are similar to the ones obtained for the translation, as shown in Fig. 7. The initial speckle pattern designated by the rectangular box in Fig. 7a is almost completely preserved for a small 2% deformations (Fig. 7b), and is largely modified for the larger deformations Fig. 7c.

The resulting correlation is given in Fig. 8. As in the previous case, correlation decreased when deformation magnitude increased and when the distance to the probe decreased. We note, however, that for large deformation, the correlation showed small values, even far from the probe.

6.2. Motion estimation accuracy

This section reports the influence of previous decorrelation results on the accuracy of two motion estimation methods based on region matching. We compared classical block matching (BM), a reference method used in the field of motion estimation, and the bilinear deformable block matching (BDBM).

6.2.1. Translation

Fig. 9 displays the mean error MEM as a function of displacement magnitudes and depth D . For polar data and for BM and BDBM (Fig. 9a and b), the error increased with translation magni-

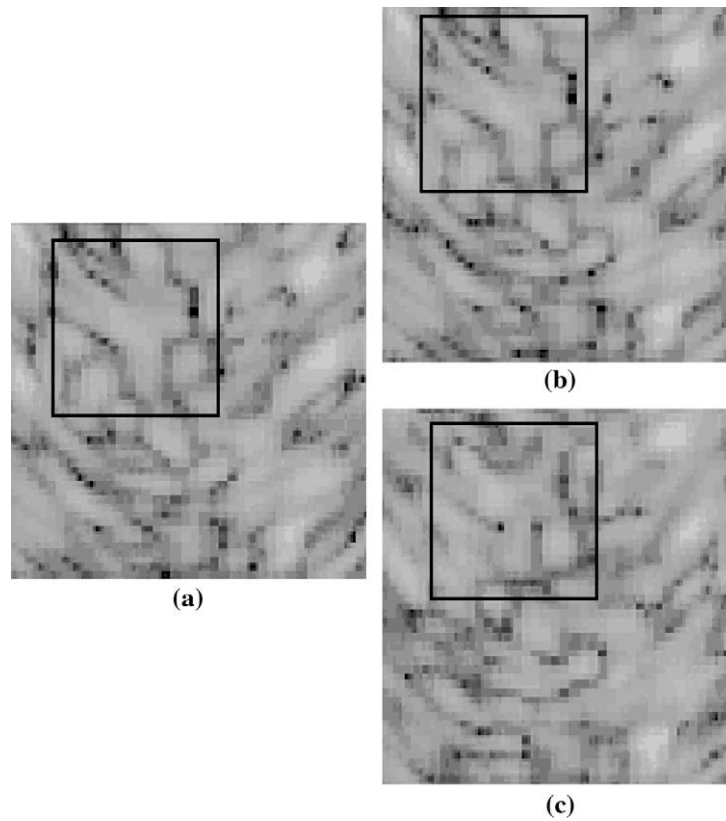


Fig. 7. (a) Simulated polar image corresponding to the tissue in initial position. A well-defined speckle pattern is designated by the black rectangle. (b) Image obtained after a 2% deformation has been applied to the tissue. Decorrelation is very low and the initial speckle pattern may be easily tracked. (c) Image obtained after a 10% deformation has been applied to the tissue. Because the deformation is larger, important decorrelation takes place and the initial speckle pattern is almost lost.

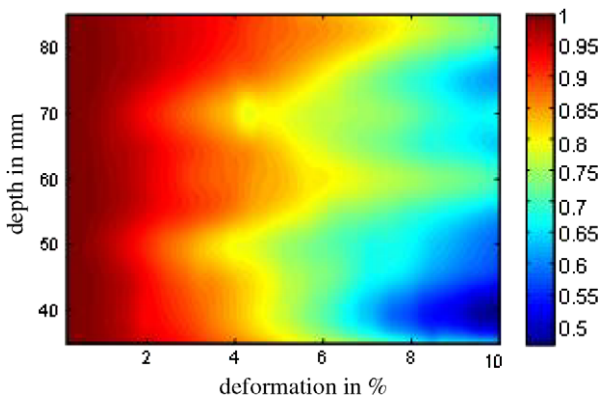


Fig. 8. Normalized correlation for the deformation, as a function of depth from the probe and deformation magnitude.

tude and the error was larger near the probe ($D = 35$ mm), consistent with decorrelation being greater in this area. We note that BDBM improved accuracy in this latter case. The same tendencies can be observed with cartesian data (Fig. 9c and d). However, it should be noted that the error for cartesian data was larger than for polar data, for both BM and BDBM.

Fig. 10 displays the standard deviation SDEM as a function of translation magnitude and depth D . As compared to the mean error MEM, two similar tendencies appear:

- In all cases, SDEM increased with translation magnitude and was greater near the probe.

- SDEM was smaller for polar data (Fig. 10a and b) than for cartesian data (Fig. 10c and d).

However, a larger difference can be observed between BM and BDBM: in all cases, the standard deviation associated with BDBM (Fig. 10b and d) was smaller than the standard deviation corresponding to BM (Fig. 10a and c).

6.2.2. Deformation

Fig. 11 displays the mean error MEM as a function of deformation magnitude and depth D . The results associated with polar data (Fig. 11a and b) shows that BM and BDBM were very close. In both cases, the MEM error increased with deformation magnitude. As opposed to translation, depth had little influence on the error. This is related to the deformation magnitude and to the applied deformation being centered on the tissue region. The maximum axial deformation (10%) applied to the 5-mm-long tissue thus corresponds to a maximum local displacement of 0.5 mm.

As shown in Fig. 11c, the combined effect of decorrelation and sectorial geometry yielded large MEM error for cartesian data, as compared to polar data when BM was applied. In contrast, Fig. 11d indicates that BDBM was able to noticeably compensate these effects and yielded an improved accuracy at all depths, particularly for the larger deformations (i.e., from 4%).

Fig. 12 displays the standard deviation SDEM as a function of deformation magnitude and the depth D . From Fig. 12, various observations similar to the MEM error above can be made:

- For polar data (Fig. 12a and b), BM and BDBM show similar results. SDEM was small and increased with deformation magnitude.

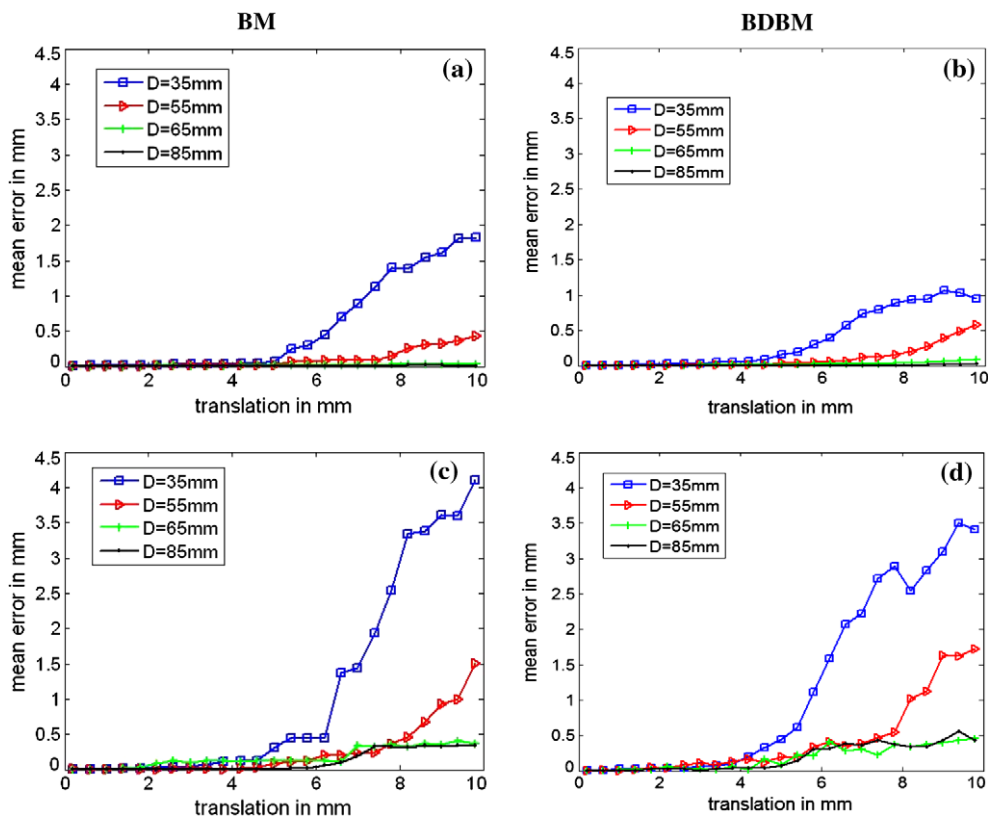


Fig. 9. Error associated with translation. Row 1: Mean error obtained when motion estimation is applied on polar data using: (a) block matching (BM), (b) bilinear deformable block matching (BDBM). Row 2: Mean error obtained when motion estimation is applied on cartesian data using: (c) block matching (BM) and (d) bilinear deformable block matching (BDBM).

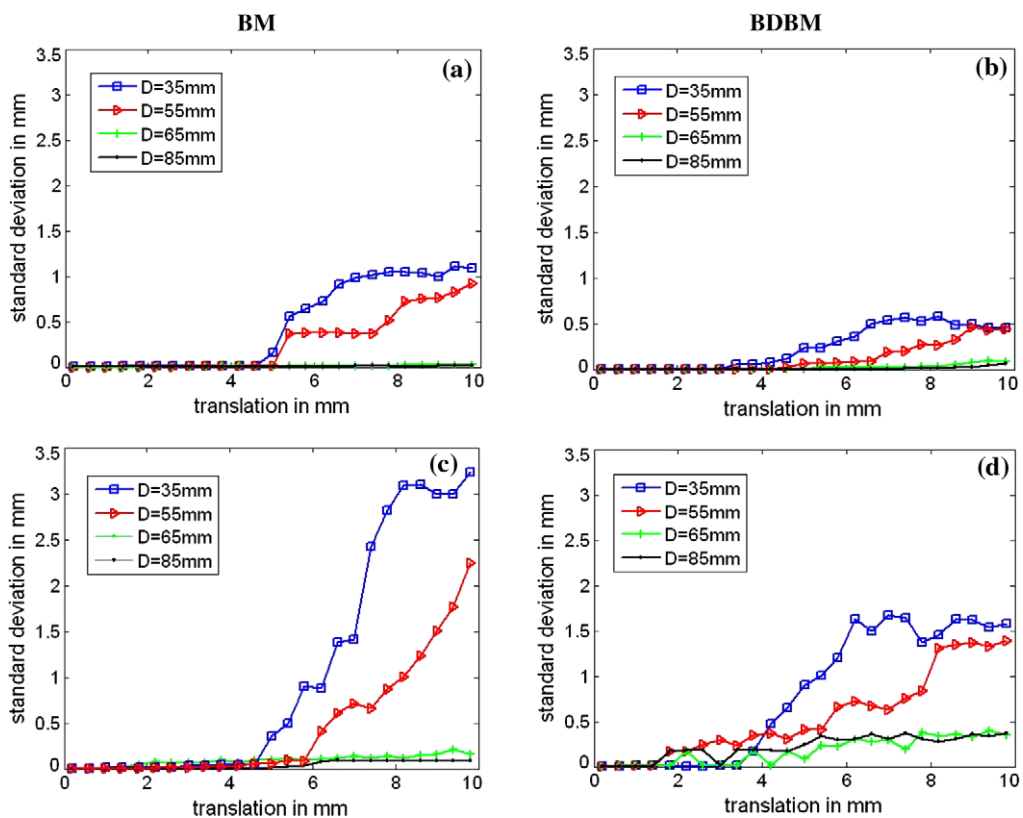


Fig. 10. Standard deviation associated with translation. Row 1: Standard deviation obtained when motion estimation is applied on polar data using: (a) block matching (BM), (b) bilinear deformable block matching (BDBM). Row 2: Standard deviation obtained when motion estimation is applied on cartesian data using: (c) block matching (BM) and (d) bilinear deformable block matching (BDBM).

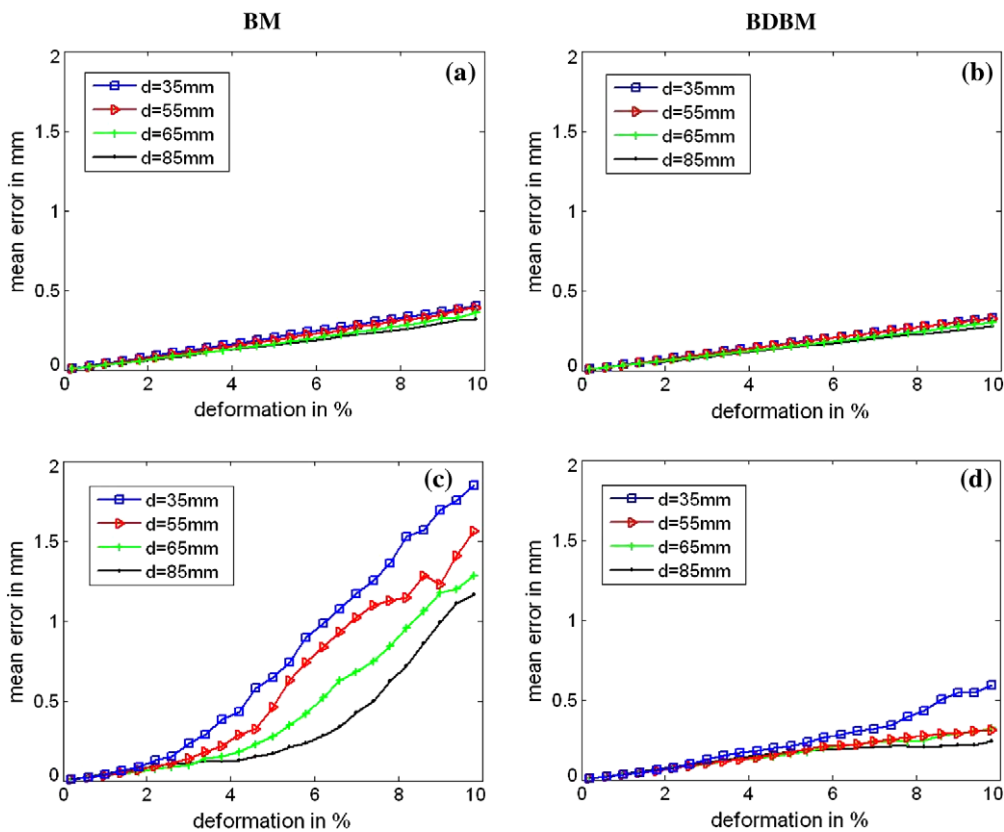


Fig. 11. Error associated with deformation. Row 1: Mean error obtained when motion estimation is applied on polar data using: (a) block matching (BM), (b) bilinear deformable block matching (BDBM). Row 2: Mean error obtained when motion estimation is applied on cartesian data using: (c) block matching (BM) and (d) bilinear deformable block matching (BDBM).

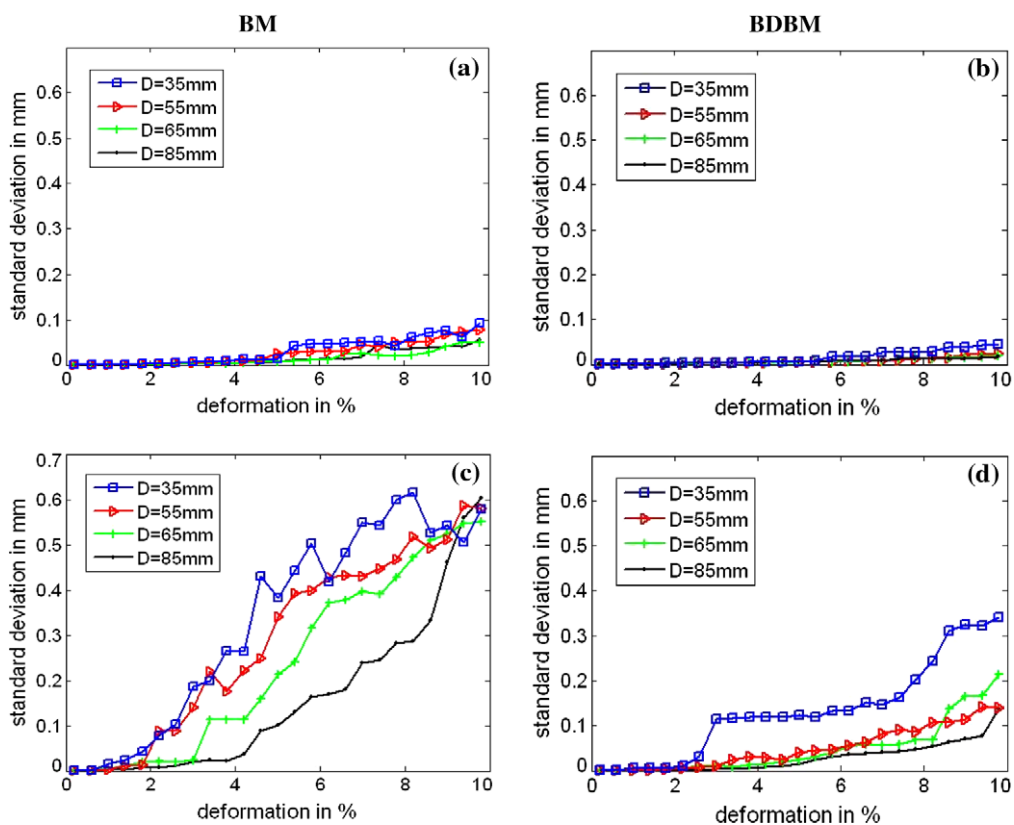


Fig. 12. Standard deviation associated with deformation. Row 1: Standard deviation obtained when motion estimation is applied on polar data using: (a) block matching (BM), (b) bilinear deformable block matching (BDBM). Row 2: Standard deviation obtained when motion estimation is applied on cartesian data using: (c) block matching (BM) and (d) bilinear deformable block matching (BDBM).

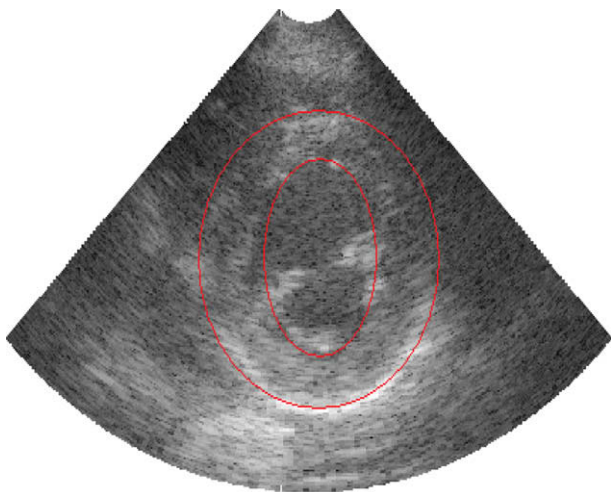


Fig. 13. Parasternal short axis view of left ventricle. The red contours show the myocardium borders (excluding the papillary muscles). (For interpretation of the references to colour in this figure legend, the reader is referred to the web version of this article.)

- SDEM was much larger for cartesian data when BM was used (Fig. 12a). BDBM noticeably improved this situation (Fig. 12d).

7. Results from echocardiographic data

A preliminary evaluation of the previous framework is performed from an echocardiographic sequence. Data were acquired using a Toshiba Powervision 6000 (Toshiba Medical Systems Europe, Zoetermeer, The Netherlands) equipped with a 3.25-MHz probe and acquired on a normal subject with a frame rate of 61 fps. Each image was composed of 120 lines with an angular interval of 0.76° , corresponding to a 90-degree explored sector.

As in the simulation, motion was estimated using the two block matching methods (BM and BDBM) and applied to cartesian and polar data. To conduct the experiment with varying motion amplitude, the estimation was made between a fixed reference image (frame one of the sequence) and the subsequent images (i th frame in the sequence). The sequence studied was located in middle systole for the parasternal short axis of the left ventricle (as shown in Fig. 13), corresponding to six frames of the data set, itself corresponding to a mean displacement magnitude increasing up to 10 mm.

As ground truth reference motion was not available for these data, the motion estimation results were evaluated by comparing the reference image and the subsequent images after motion compensation. This comparison was made on a 10×30 -mm rectangular region of interest corresponding to the myocardium (this region² is depicted as a blue rectangle in Figs. 14 and 15). The comparison was quantified by computing the normalized correlation (NCC).

Fig. 14a and b shows the displacement field corresponding to the second frame obtained with BM and BDBM from polar data and superimposed on the reference image. Fig. 14c and d provides a detailed view of the estimated displacement field in a region included in the myocardium and shown as the blue window on the complete images (Fig. 14a and b). It can be observed that the field corresponding to BDBM is somewhat smoother than for BM, which produces higher amplitudes in the upper right region.

Fig. 14e displays the normalized correlation as a function of the time interval. For BM and BDBM, the NCC decreased with motion magnitude, which is consistent with the results observed in the simulation. Moreover, BDBM appears to be more accurate than BM, since it yielded higher NCC at all time intervals (NCC is in the interval (0.98–0.55) for BDBM and (0.65–0.2) for BM).

Fig. 14 shows the corresponding results for cartesian data. Fig. 15c and d indicates that the field provided by BDBM was somewhat smoother than for BM. Fig. 15e shows that NCC decreased with motion magnitude, both for BM and BDBM. As with the polar data, we observe that the BDBM provided better results than BM, yielding higher NCC at any time interval (NCC is in the interval (0.98–0.2) for BDBM and (0.45–0.02) for BM).

Comparing Figs. 14e and 15e also show that the results obtained from polar data appear to be more accurate than the results derived from cartesian data, whatever the estimation method: BDBM yielded a NCC in the range (0.98–0.55) for polar data versus (0.98–0.2) for cartesian data. Similarly, BM provided a NCC in the range (0.65–0.2) for polar data versus (0.45–0.02) for cartesian data. We also note that the improvement brought by BDBM over BM was greater for cartesian data. This is consistent with the results shown from the simulation.

8. Conclusion

This paper reports the investigation of the influence of echographic image formation parameters (sectorial geometry, spatially varying PSF) on speckle tracking using realistic simulations.

These simulations first showed the influence of the decorrelation induced by the system for simple motions (translation and incompressible deformation). The decorrelation is a spatially variant phenomenon, which depends on the position of the imaged tissue region relative to the probe: for translation and deformation, decorrelation is more important for regions of the tissue located close to the probe. Moreover, the results indicate that decorrelation may even appear for translation, which usually had not been considered in previous studies. This phenomenon is limited to high-amplitude translations in regions located close to the probe.

We quantified speckle tracking accuracy using a conventional block matching algorithm and a bilinear deformable block matching algorithm applied to cartesian and polar data. The results show that errors are larger for the usual cartesian data whatever the estimation algorithm: for axial translations in the range 0–10 mm and conventional block matching, the maximum error is 4.2 mm when using cartesian data and 1.8 mm for polar data. The corresponding errors are 1.8 mm and 0.4 mm for an applied deformation from 0 to 10%. In the same way, the bilinear deformable block matching yields a maximum error of 3.6 mm (cartesian data) and 1.2 mm (polar data) for translation. Regarding deformation, the error is 0.7 mm (cartesian data) and 0.3 mm (polar data). This is related to the sectorial geometry of echocardiographic acquisition, which induces a sparser sampling far from the probe.

We also show that the accuracy of tracking is significantly improved by using the bilinear deformable block matching algorithm. This improvement was found to be more significant with cartesian data and for deformation: the maximum error indeed drops from 1.8 to 0.7 mm in this case whereas it decreases from 0.4 mm to 0.3 mm in the case of polar data. This result is consistent with the purpose of the bilinear deformable block matching which was designed to compensate for local deformation of the speckle structure. For translation, the maximum error decreases from 4.2

² For interpretation of color in Figs. 14 and 15, the reader is referred to the web version of this article.

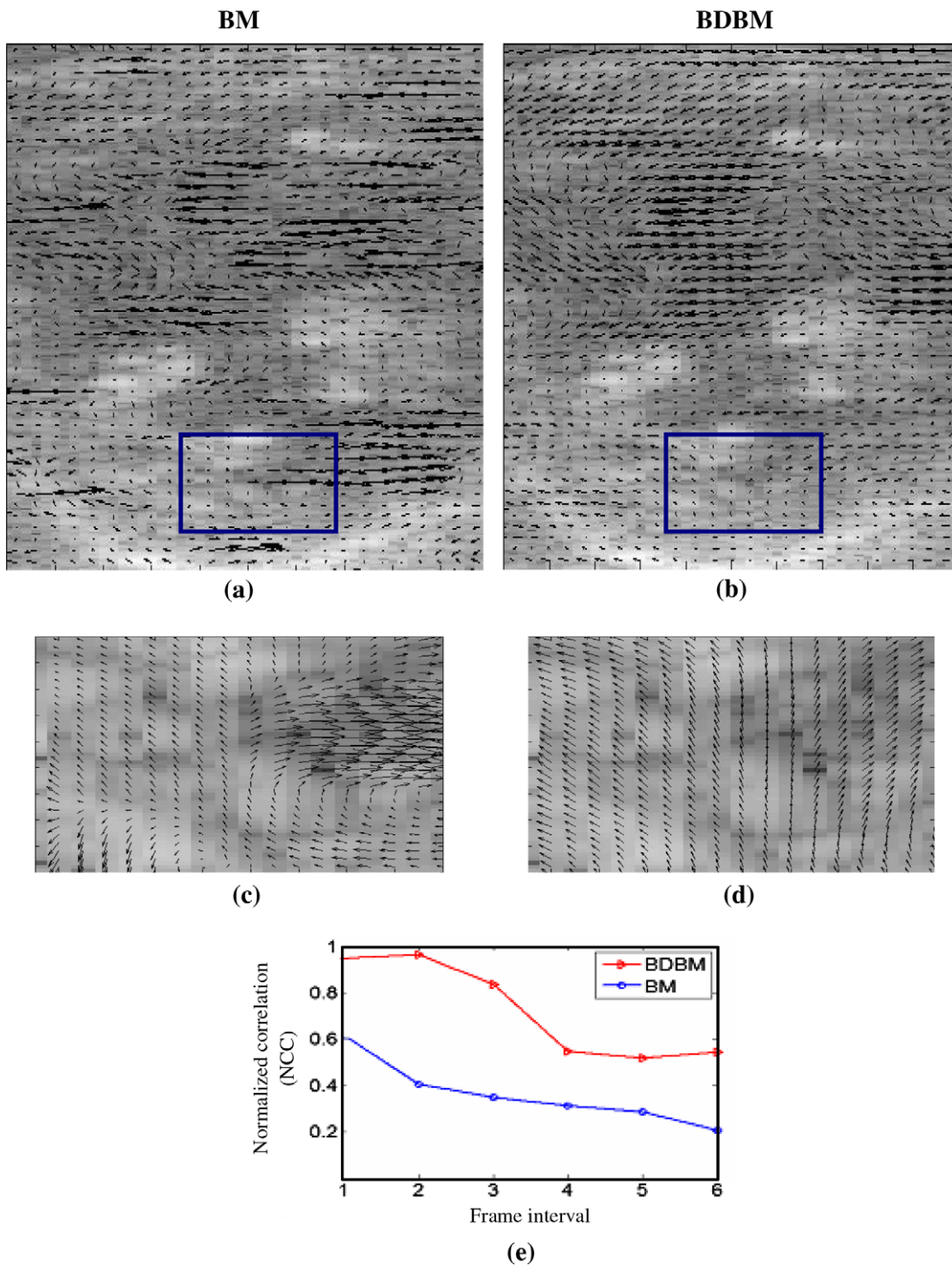


Fig. 14. Motion field estimated from polar data. Column 1: (a) motion field estimated using block matching (BM) superimposed on the whole reference frame. The blue rectangle indicates a region of interest (c) details of the motion field in the region of interest. Column 2: (b) motion field estimated using bilinear deformable block matching (BDBM) superimposed on the whole reference frame. The blue rectangle indicates a region of interest (d) details of the motion field in the region of interest. (e) Normalized correlation (NCC) between the reference image and the subsequent motion-compensated images as a function of the inter-frame interval.

to 3.6 mm when using cartesian data, whereas it decreases from 1.8 to 1.2 mm for polar data.

Overall, this simulation study suggests that speckle tracking from echocardiographic data should be performed from unconverted polar data. Whenever these data are not available, the track-

ing on the usual scan-converted cartesian data is markedly improved by using deformable block matching.

Verifying these conclusions on real echocardiographic data is difficult, since ground truth reference motion is not available. In this experiment, this was done by computing the correlation be-

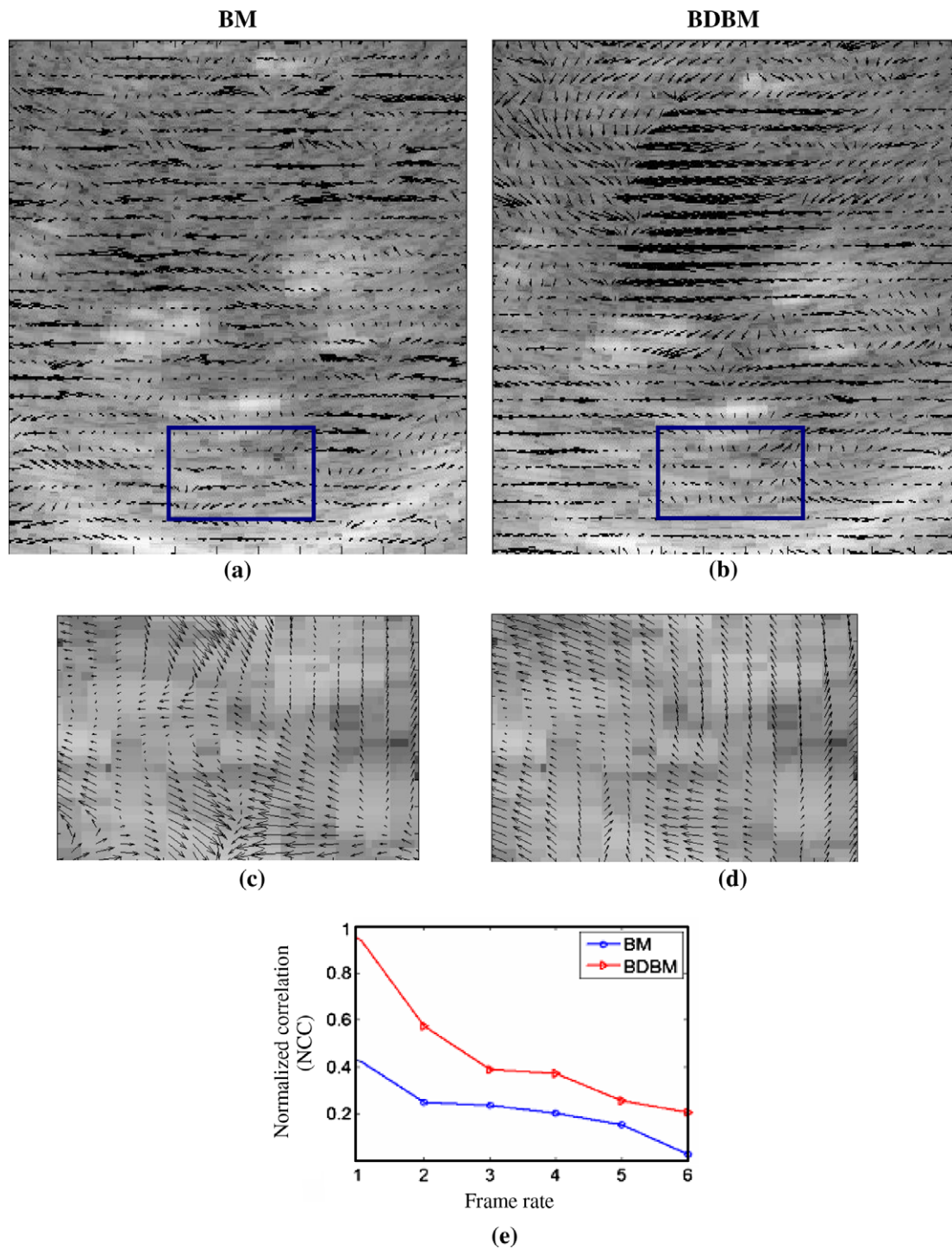


Fig. 15. Motion field estimated from cartesian data. Column 1: (a) motion field estimated using block matching (BM) superimposed on the whole reference frame. The blue rectangle indicates a region of interest. (c) Details of the motion field in the region of interest. Column 2: (b) motion field estimated using bilinear deformable block matching (BDBM) superimposed on the whole reference frame. The blue rectangle indicates a region of interest (d) and details of the motion field in the region of interest. (e) Normalized correlation (NCC) between the reference image and the subsequent motion-compensated images as a function of the inter-frame interval.

tween a reference image and the subsequent image after motion compensation. The results obtained in this way confirmed the results obtained from the simulations.

References

[1] P. Baraldi, A. Sarti, C. Lamberti, A. Prandini, F. Sgallari, Evaluation of differential optical flow techniques on synthesized echo images, *IEEE Transactions on Biomedical Engineering* 43 (3) (1996) 259–272.

[2] G.E. Mailloux, A. Bleau, M. Bertrand, P. Petitclerc, Computer analysis of heart motion from two-dimensional echocardiograms, *IEEE Transactions on Biomedical Engineering* 34 (5) (1987) 356–364.

[3] G.E. Mailloux, F. Langlois, P. Simard, M. Bertrand, Restoration of the velocity field of the heart from two-dimensional echocardiograms, *IEEE Transactions on Medical Imaging* 8 (1989) 143–153.

[4] V. Behar, D. Adam, P. Lysyansky, Z. Friedman, Improving motion estimation by accounting for local image distortion, *Ultrasonics* 43 (1) (2004) 57–65.

[5] M. Suhling, M. Arigovindan, C. Jansen, P. Hunziker, M. Unser, Myocardial motion analysis from B-mode echocardiograms, *IEEE Transactions on Image Processing* 14 (4) (2005) 525–536.

- [6] V. Behar, D. Adam, P. Lysyansky, Z. Friedman, The combined effect of nonlinear filtration and window size on the accuracy of tissue displacement estimation using detected echo signals, *Ultrasonics* 41 (9) (2004) 743–753.
- [7] Q. Duan, E. Angelini, S. Homma, A.F. Laine, Validation of optical-flow for quantification of myocardial deformations on simulated RT3D ultrasound, in: *International Symposium on Biomedical Imaging*, Metro Washington, DC, USA, 2007, pp. 49–52.
- [8] C. Kontogeorgakis, M.G. Strintzis, N. Maglaveras, I. Kokkinidis, Tumor detection in ultrasound B-mode images through motion estimation using a texture detection algorithm, in: *Computers in Cardiology*, Bethesda, MD, USA, 1994, pp. 117–120.
- [9] F. Yeung, S.F. Levinson, K.J. Parker, Multilevel and motion model-based ultrasonic speckle tracking algorithms, *Ultrasound in Medicine and Biology* 24 (3) (1998) 427–442.
- [10] M.G. Strintzis, I. Kokkinidis, Maximum likelihood motion estimation in ultrasound image sequences, *IEEE Signal Processing Letters* 4 (6) (1997) 156–157.
- [11] B. Cohen, I. Dinstein, New maximum likelihood motion estimation schemes for noisy ultrasound images, *Pattern Recognition* 35 (2) (2002) 455–463.
- [12] D. Boukerroui, J. Noble, M. Brady, Velocity estimation in ultrasound images: a block matching approach, in: *Information Processing in Medical Imaging (IPMI)*, 2003, pp. 586–598.
- [13] M. Linguraru, N. Vasilyev, P. del Nido, R. Howe, Fast block flow tracking of atrial septal defects in 4D echocardiography, *Medical Image Analysis* 12 (4) (2008) 397–412.
- [14] M.A. Lubinski, S.Y. Emelianov, M. O'Donnell, Speckle tracking methods for ultrasonic elasticity imaging using short-time correlation, *IEEE Transactions on Ultrasonics, Ferroelectricity and Frequency Control* 46 (1) (1999) 82–96.
- [15] J. D'hooge, B. Bijnens, J. Thoen, F. Van de Werf, G. Sutherland, P. Suetens, Echocardiographic strain and strain-rate imaging: a new tool to study regional myocardial function, *IEEE Transactions on Medical Imaging* 21 (9) (2002) 1022–1030.
- [16] J. Luo, E.E. Konofagou, High-frame rate, full-view myocardial elastography with automated contour tracking in murine left ventricles in vivo, *IEEE Transactions on Ultrasonics, Ferroelectricity and Frequency Control* 55 (1) (2008) 240–248.
- [17] A. Basarab, P. Gueth, H. Liebgott, P. Delachartre, Two-dimensional least-squares estimation for motion tracking in ultrasound elastography, in: *International Conference of the IEEE Engineering in Medicine and Biology Society (EMBS'07)*, Lyon, France, 2007, pp. 2155–2158.
- [18] J. D'hooge, E. Konofagou, F. Jamal, A. Heimdal, L. Barrios, B. Bijnens, J. Thoen, F. Van de Werf, G. Sutherland, P. Suetens, Two-dimensional ultrasonic strain rate measurement of the human heart in vivo, *IEEE Transactions on Ultrasonics, Ferroelectricity and Frequency Control* 49 (2) (2002) 281–286.
- [19] W.-N. Lee, C.M. Ingrassia, S.D. Fung-Kee-Fung, K.D. Costa, J.W. Holmes, E.E. Konofagou, Theoretical quality assessment of myocardial elastography with in vivo validation, *IEEE Transactions on Ultrasonics, Ferroelectricity and Frequency Control* 54 (11) (2007) 2233–2245.
- [20] H. Liebgott, A. Basarab, P. Gueth, C. Cachard, P. Delachartre, Lateral RF image synthesis using a synthetic aperture imaging technique, *IEEE Transactions on Ultrasonics, Ferroelectricity and Frequency Control* 55 (9) (2008) 2097–2103.
- [21] W. Yu, P. Yan, A.J. Sinusas, K. Thiele, J.S. Duncan, Towards pointwise motion tracking in echocardiographic image sequences – comparing the reliability of different features for speckle tracking, *Medical Image Analysis* 10 (4) (2006) 495–508.
- [22] J. Meunier, M. Bertrand, Ultrasonic texture motion analysis: theory and simulation, *IEEE Transactions on Medical Imaging* 14 (2) (1995) 293–300.
- [23] S.K. Alam, J. Ophir, Reduction of signal decorrelation from mechanical compression of tissues by temporal stretching: applications to elastography, *Ultrasound in Medicine and Biology* 23 (1) (1997) 95–105.
- [24] R.L. Maurice, M. Bertrand, Lagrangian speckle model and tissue-motion estimation – theory, *IEEE Transactions on Medical Imaging* 18 (7) (1999) 593–603.
- [25] P. Chaturvedi, M.F. Insana, T.J. Hall, 2-D companding for noise reduction in strain imaging, *IEEE Transactions on Ultrasonics, Ferroelectricity and Frequency Control* 45 (1) (1998) 179–191.
- [26] Y. Zhu, P. Chaturvedi, M.F. Insana, Strain imaging with a deformable mesh, *Ultrasonic Imaging* 21 (2) (1999) 127–141.
- [27] C. Pellot-Barakat, F. Frouin, M.F. Insana, A. Herment, Ultrasound elastography based on multiscale estimations of regularized displacement fields, *IEEE Transactions on Medical Imaging* 23 (2) (2004) 153–163.
- [28] S. Langeland, J. D'hooge, H.G. Torp, B. Bijnens, P. Suetens, Comparison of time-domain displacement estimators for two-dimensional RF tracking, *Ultrasound in Medicine and Biology* 29 (8) (2003) 1177–1186.
- [29] A. Basarab, W. Aoudi, H. Liebgott, D. Vray, P. Delachartre, Parametric deformable block matching for ultrasound imaging, in: *IEEE International Conference on Image Processing (ICIP'07)*, San Antonio, Texas, USA, 2007, pp. 429–432.
- [30] J.A. Jensen, Simulation of advanced ultrasound systems using Field II, *International Symposium on Biomedical Imaging* 1 (2004) 636–639.
- [31] P.R. Stepanishen, The time-dependent force and radiation impedance on a piston in a rigid infinite planar baffle, *Journal of the Acoustical Society of America* 49 (3) (1971) 841–849.
- [32] G.E. Topholme, Generation of acoustic pulses by baffled plane pistons, *Mathematika* 16 (1969) 209–224.
- [33] R.F. Wagner, S.W. Smith, J.M. Sandrik, H. Lopez, Statistics of speckle in Ultrasound B-scans, *IEEE Transactions on Sonics and Ultrasonics* 30 (3) (1983) 156–163.
- [34] B. Touil, O. Bernard, D. Friboulet, Motion decorrelation in echocardiography: analysis from realistic simulations, *International Symposium on Biomedical Imaging* (2008) 1469–1472.
- [35] A. Basarab, H. Liebgott, F. Morestin, A. Lyschchik, T. Higashi, R. Asato, P. Delachartre, A method for vector displacement estimation with ultrasound images and its application for thyroid nodular disease, *Medical Image Analysis* 12 (3) (2008) 259–274.
- [36] P. Delachartre, H. Liebgott, F. Lacouture, F. Morestin, A. Lyschchik, T. Higashi, R. Asato, Bilinear modelling and estimation of displacement for thyroid cancer elasticity imaging, *Traitement du Signal* 23 (3/4) (2006) 235–245.